Available online at www.sciencedirect.com
SCIENCE DIRECT
Earth and Planetary Science Letters 234 (2005) 27–38
EPSL
www.elsevier.com/locate/epsl

# Thin shell dynamo models consistent with Mercury's weak observed magnetic field

Sabine Stanley[a,*], Jeremy Bloxham[a,1], William E. Hutchison[b,2], Maria T. Zuber[b,2]

[a]Department of Earth and Planetary Sciences, Harvard University, Cambridge, Massachusetts 02138, United States
[b]Department of Earth, Atmospheric and Planetary Sciences, Massachusetts Institute of Technology, Cambridge, Massachusetts 02139, United States

Received 3 September 2003; received in revised form 28 January 2005; accepted 18 February 2005
Available online 22 April 2005
Editor: V. Courtillot

**Abstract**

Energetic and magnetostrophic balance arguments show that a dynamo source for Mercury's observed magnetic field is problematic if one expects an Earth-like partitioning of toroidal and poloidal fields. We perform 3-dimensional numerical dynamo simulations to determine if a thin shell dynamo geometry for Mercury could produce non-Earth-like magnetic field partitioning and therefore provide a possible explanation of Mercury's weak observed dipole signature. We examine the ratio of the dipole field at the core–mantle boundary to the toroidal field in the core for various shell thicknesses and Rayleigh numbers and find that some thin shell dynamos can produce magnetic fields with Mercury-like dipolar field intensities. In these dynamos, the toroidal field is produced more efficiently through differential rotation than the poloidal field is produced through upwellings interacting with the toroidal field. The poloidal field is also dominated by smaller-scale structure which was not observable by the Mariner 10 mission, compared to the dipole field.


*PACS:* 91.25.Cw; 96.30.Dz
*Keywords:* Mercury; magnetic field; dynamo; numerical modeling

## 1. Introduction

Mariner 10's observations during the first and third flybys of Mercury in 1974–1975 revealed the presence of a magnetic field of internal origin [1,2]. The inferred magnetic dipole moment of about 300 $\mathrm{nT}-R_M^3$ ($1R_M=2440\ km$) is not well constrained due to the spatial distribution and limited quantity of

* Corresponding author. Tel.: +1 617 495 8986; fax: +1 617 495 7660.
*E-mail addresses:* stanley@geophysics.harvard.edu (S. Stanley), jeremey_bloxham@harvard.edu (J. Bloxham), hutch@mit.edu (W.E. Hutchison), mtz@mit.edu (M.T. Zuber).
[1] Tel.: +1 617 495 9517.
[2] Tel.: +1 617 253 6397.

0012-821X/$ - see front matter © 2005 Elsevier B.V. All rights reserved.
doi:10.1016/j.epsl.2005.02.040

the data [3], but even with this uncertainty, the inferred field strength appears problematic for all typical sources of planetary magnetic fields.

The observed magnetic field strength is much too large to be explained by induction effects from solar wind currents on the premise that an induced field should not be larger than the inducing field. Impact magnetization is an unlikely candidate since a global dipolar field would not be the expected resulting morphology. One possibility is that the dipole field is due to crustal remanent magnetization from a dynamo operating in Mercury's past. If this is the case, then Mercury's crustal magnetism is quite different from that of Earth and Mars where crustal magnetic fields are short wavelength (i.e. non-dipolar) features. Runcorn's theorem [4] showed that a uniform spherical shell magnetized by an internal field cannot be the source of the dipole signature, however a planet is capable of producing a dipole remanent field if inhomogeneities exist in the magnetized shell. Stephenson [5] and Srnka [6] suggested variations in magnetic permeability between the shell and free space or the interior as a possible inhomogeneity, and more recently, Aharonson et al. [7] showed that variations in crustal thickness due to laterally varying external temperature gradients at Mercury could be a source of inhomogeneity. In both cases, a dipolar field can be produced from the crustal magnetism, but it is difficult to reconcile the field's strength. In order to explain the field's intensity, Mercury's crust must contain minerals capable of sustaining high specific magnetizations (similar to the magnetizations needed to explain Mars' crustal field), or Mercury's past dynamo must have produced a field much more intense than Earth's (which is unlikely). Reversals must also be at a minimum since they diminish the resultant field strength. Although it appears difficult to explain Mercury's field via crustal remanence, this possibility cannot be ruled out.

The possibility we will consider in the rest of this study is whether the field could be due to an active dynamo. Before the field's discovery, this wasn't considered likely since Mercury's small size suggested the planet should have cooled efficiently and hence completely frozen its iron core, negating the possibility of current dynamo action. However, the recent discovery by the Galileo mission that Ganymede has an active dynamo [8] suggests that it may not be so unusual for a Mercury-size body to possess a dynamo. Recent Earth-based radar measurements of Mercury's librations in longitude [9] have demonstrated that the core and mantle of Mercury are decoupled, and hence that the core must be at least partially fluid. This provides the basic necessary (although by no means sufficient) condition for an active dynamo to be the source of the magnetic observations. What is unknown is whether this fluid region contains the necessary complex 3-D motions required to maintain magnetic field generation against ohmic decay.

Although early thermal evolution models demonstrated that it is difficult to keep a pure iron core in Mercury from freezing totally [10], Stevenson et al. [11] showed that the core can remain at least partially molten if it contains a small concentration of a light element such as sulfur. In the models studied, plausible sulfur concentrations of 1–5% resulted in thin liquid outer cores surrounding relatively large solid inner cores. The inner to outer core radius ratios were in the range 0.74–0.96. These values are much larger than Earth's radius ratio of 0.35. Other thermal evolution models that, in addition to a light element, also incorporate tidal heating [12], pressure and temperature dependent rheology [13] and the magmatic and tectonic evolution of Mercury [14] show that outer liquid layers are easily produced for a wide range of parameter values.

An active dynamo source for Mercury's field has been viewed as problematic because of discrepancies between the observed field's magnitude and theoretical estimates of the magnetic field strength produced by an Earth-like dynamo (Earth-like dynamo would produce a much stronger field than observed). Because the available typical sources for Mercury's magnetic field are problematic, alternatives such as a thermoelectric dynamo [15,16] have been considered.

Theoretical modeling and Earth-based radar observations are in agreement that Mercury contains at least a partially molten core. Although the radar measurements cannot determine the size of the solid inner core, the thermal evolution models show that a wide range of inner core radii is possible. The earlier models favored a relatively large solid inner core, and although the more recent models have relaxed this constraint somewhat, they still allow for large solid inner cores. In this paper we investigate whether

Mercury's weak surface magnetic field is the result of dynamo action in a thin shell geometry. This geometry is different from the thick shell geometry of Earth's core which may lead to differences in the magnetic fields they produce. We use numerical dynamo modeling to study thin shell dynamos and examine whether they can produce magnetic fields capable of explaining the observations at Mercury.

## 2. Magnetic field strength expected from a dynamo

There are two independent methods for estimating the magnetic field strength generated by a dynamo. The first method (energy balance) involves balancing the gravitational energy release driving the dynamo and the ohmic energy dissipated through electrical currents. Using thermal evolution models for Mercury to estimate the gravitational energy, magnetic field strengths on the order of $10^5$–$10^7$ nT are obtained [12,15]. The second method (magnetostrophic balance) relies on assuming that Mercury's dynamo operates in the strong-field regime where the Lorentz force balances the Coriolis force. This results in an estimate for the magnetic field of $B = \sqrt{2\Omega\rho Re_M/\sigma}$ where $B$ is the magnetic field, $\Omega$ is the rotation rate of the planet, $\rho$ is density, $\sigma$ is electrical conductivity and $Re_M = UL/\eta$ is the magnetic Reynolds number ($\eta$ is the magnetic diffusivity, $U$ is a typical velocity scale and $L$ is a typical length scale). Using magnetic Reynolds numbers on the order of 10–1000 (10 is the minimum $Re_M$ value for dynamo action), we obtain an estimate for the field strength in the same range as was found using energetic arguments.

It is possible that Mercury's dynamo is an 'energy limited dynamo' in which magnetostrophic balance does not occur [17] and therefore does not provide a valid estimate for the magnetic field. However in this case, one must also find a reason to reject the independent energy balance estimate. Since this estimate is based on numerical thermal evolution calculations, which depend on some parameters that are not well known (such as the concentration of light element in the core), it may not be unreasonable to reject this method as well. We however, find comfort in the fact that both methods produce similar field values for Mercury and we choose to examine whether it is possible for a dynamo in magnetostrophic balance to produce Mercury's weak dipolar field.

The magnetic field estimate provided by these two methods does not immediately conflict with the observed field value since the estimate is of the field strength in the fluid core, rather than at some distance outside the core where the observations are made. Because the magnetic field is divergence-free ($\nabla \cdot \mathbf{B} = 0$), we can represent the core field in spherical harmonics using the toroidal–poloidal decomposition:

$$\mathbf{B} = \mathbf{B}_T + \mathbf{B}_P = \nabla \times T\hat{\mathbf{r}} + \nabla \times (\nabla \times P\hat{\mathbf{r}}), \qquad (1)$$

where $\mathbf{B}_T$ and $\mathbf{B}_P$ are the toroidal and poloidal field components, respectively, $T$ and $P$ are the toroidal and poloidal scalars, respectively, and $\hat{\mathbf{r}}$ is a unit vector in the radial direction. Since the toroidal field has no radial component, it is not observable outside the conducting core and only the poloidal field is measured outside the dynamo generation region. The magnetic field estimate given by the energy and magnetostrophic balance arguments pertains to the combination of the toroidal and poloidal field components in the core. If the observed dipole component of the field is downward continued to the core mantle boundary, then it is not large enough to satisfy the energy and magnetostrophic balance estimates. This means that the toroidal field or the non-dipolar poloidal field in the core must do so. The dynamo models we present in this paper maintain magnetostrophic balance through the toroidal field. We therefore use this choice throughout the rest of this paper. For dynamo models that maintain magnetostrophic balance via the non-dipolar poloidal field and have a weaker dipolar field, see Kutzner and Christensen [18]. Since we assume the toroidal field maintains magnetostrophic balance, the dipole poloidal field is not restricted in magnitude and can be much weaker than the toroidal field.

The problem arises when one compares the dipole field strength at Mercury's core–mantle boundary to the toroidal field strength in Mercury's core (estimated using the energy or magnetostrophic balance arguments). The ratio of these fields is $B_{Dip}/B_T \approx 10^{-2}$–$10^{-4}$. By carrying out a similar analysis of Earth's dynamo, we find $B_{Dip}/B_T \approx 10^{-1}$. This is where a dynamo solution for Mercury's field

becomes problematic since it appears that Mercury's dynamo produces a much smaller $B_{\mathrm{Dip}}/B_{\mathrm{T}}$ ratio than Earth's dynamo and it is unclear why this should be the case.

We wish to examine whether a thin shell dynamo could explain the much smaller $B_{\mathrm{Dip}}/B_{\mathrm{T}}$ ratio found for Mercury. One possibility is that the ratio of poloidal field to toroidal field in the core ($B_{\mathrm{P}}/B_{\mathrm{T}}$) may be smaller if the generation of toroidal field is more efficient than the generation of poloidal field. Another possibility is that the poloidal field may be dominated by smaller scale structure than the dipole leading to a smaller $B_{\mathrm{Dip}}/B_{\mathrm{P}}$ ratio. This would imply that projecting the dipole field observed by Mariner 10 to the CMB does not provide a good estimate for the CMB poloidal field at Mercury (unlike the Earth case where it is believed the dipole component at the CMB does provide a good estimate for the poloidal field strength there). We examine both of these possibilities in the following sections.

## 3. Numerical model

We use the Kuang and Bloxham [19,20] 3-dimensional numerical dynamo model to study magnetic field generation in a thin, spherical, rotating, Boussinesq, electrically conducting fluid shell surrounding a solid electrically conducting inner core. By using the radius of the core ($r_{\mathrm{o}}$) as a length scale, the magnetic diffusion time ($\tau=r_{\mathrm{o}}^2/\eta$ where $\eta$ is the magnetic diffusivity) as a timescale, a magnetostrophic balance estimate $B=\sqrt{2\Omega\rho/\sigma}$ as the magnetic field scale and $h_{\mathrm{T}}r_{\mathrm{o}}$ (where $h_{\mathrm{T}}$ is the temperature gradient responsible for the incoming heat flux at the inner core boundary) as a temperature scale, we obtain the non-dimensional equations governing the system:

$$Ro\left(\frac{\partial}{\partial t}+\mathbf{v}\cdot\nabla\right)\mathbf{v}+\hat{\mathbf{z}}\times\mathbf{v}=-\nabla p+\mathbf{J}\times\mathbf{B}+\frac{Ra}{(1-r_{\mathrm{io}})^2}\Theta\mathbf{r}+E(1-r_{\mathrm{io}})^2\nabla^2\mathbf{v}, \tag{2}$$

$$\left(\frac{\partial}{\partial t}-\nabla^2\right)\mathbf{B}=\nabla\times(\mathbf{v}\times\mathbf{B}), \tag{3}$$

$$\left(\frac{\partial}{\partial t}-q_\kappa\nabla^2\right)\Theta=-\mathbf{v}\cdot\nabla(T_0(r)+\Theta), \tag{4}$$

$$\nabla\cdot\mathbf{B}=0, \tag{5}$$

$$\nabla\cdot\mathbf{v}=0. \tag{6}$$

Here $\mathbf{v}$, $\mathbf{B}$, $\Theta$ are the velocity, magnetic and temperature perturbation fields respectively, $T_0(r)$ is a reference temperature state that matches the boundary conditions and would be present in the absence of convection, the total temperature $T=T_0(r)+\Theta$, $p$ is the modified pressure, $\mathbf{J}$ is the current density and $\hat{\mathbf{z}}$ is a unit vector in the direction of the rotation axis so the rotation vector $\mathbf{\Omega}=\Omega\hat{\mathbf{z}}$. The non-dimensional parameters in the above equations are the magnetic Rossby number $Ro$, the Ekman number $E$, the inner core to total core radius ratio $r_{\mathrm{io}}$, the Rayleigh number $Ra$ and the magnetic Prandtl number $q_\kappa$ which are given by:

$$Ro\equiv\frac{\eta}{2\Omega r_{\mathrm{o}}^2}, \tag{7}$$

$$E\equiv\frac{\nu}{2\Omega r_{\mathrm{o}}^2(1-r_{\mathrm{io}})^2}, \tag{8}$$

$$r_{\mathrm{io}}\equiv\frac{r_{\mathrm{i}}}{r_{\mathrm{o}}}, \tag{9}$$

$$Ra\equiv\frac{\alpha_{\mathrm{T}}g_{\mathrm{o}}h_{\mathrm{T}}r_{\mathrm{o}}^2(1-r_{\mathrm{io}})^2}{2\Omega\eta}, \tag{10}$$

$$q_\kappa=\frac{\kappa}{\eta}, \tag{11}$$

where $\nu$ is the kinematic viscosity, $\alpha_{\mathrm{T}}$ is the thermal expansion coefficient, $g_{\mathrm{o}}$ is the gravitational acceleration at $r_{\mathrm{o}}$, and $\kappa$ is the thermal diffusivity. The term $r_{\mathrm{o}}(1-r_{\mathrm{io}})$ is just the fluid outer core shell thickness ($d=r_{\mathrm{o}}-r_{\mathrm{i}}$) written in terms of our control parameters. Note that the definition of the Rayleigh number here is different than is used for example in mantle convection problems where buoyancy forces must overcome viscous forces in order to convect. In core convection, where viscous forces are small and Coriolis forces are strong, the buoyancy force must overcome the strong Coriolis

force in order for convection to begin and hence the Rayleigh number is defined in terms of this force balance.

We use fixed heat flux boundary conditions on the temperature, and finite electrically conducting boundary conditions on the magnetic field. For the velocity field, we use impenetrable and viscous stress-free boundary conditions. Although stress-free boundary conditions are not technically correct for the problem, we use them for the same reason that Kuang and Bloxham [19,20] do, namely that since numerical dynamo models must use Ekman numbers that are much larger than appropriate for planetary cores, we decrease the effects of the Ekman boundary layers in our models by choosing stress-free boundaries. This choice results in $\alpha\omega$ numerical dynamos that have torsional oscillations about a Taylor state (see Kuang and Bloxham [19]). There is evidence of torsional oscillations in Earth's core [21] suggesting this boundary value choice may produce dynamos that operate in more of a planetary-like state, unlike dynamo models with no-slip boundary conditions, in which the torsional oscillations are damped out by the strong viscous forces in the large Ekman layers. In order to work at highly supercritical Rayleigh numbers (appropriate for planetary cores), we employ similar hyper-diffusivities as [20]. For more detailed information on the equations; approximations and numerical method refer to [20].

Due to our choice of length scale in the non-dimensionalization, the buoyancy term scales with the non-dimensional grouping $Ra/(1-r_{\mathrm{io}})^2$ which we shall refer to as the modified Rayleigh number ($Ra_{\mathrm{m}}$,) and the viscous term scales with $E(1-r_{\mathrm{io}})^2$ which we shall refer to as the modified Ekman number $E_{\mathrm{m}}$. We study only the effects of varying the inner core radius and modified Rayleigh number on the solutions and therefore, keep all other parameters the same for all models. We choose $Ro=E_{\mathrm{m}}=2\cdot 10^{-5}$ and $q_{\kappa}=1$. With these parameter choices, the Ekman number will vary between models with different shell thicknesses, but the modified Ekman number will remain constant and equal to the magnetic Rossby number (i.e. the inertial and viscous terms in the equations scale the same). Our parameter choice implies that all the Prandtl numbers in the system are equal to 1.

## 4. Results

Table 1 lists the control parameters and results of each model studied. Models (1)–(3) which have an Earth-like shell thickness, produce average $B_{\mathrm{Dip}}/B_{\mathrm{T}}$ ratios of about $10^{-1}$ which is the same as the theoretical estimate for Earth's dynamo. For thinner shells we observe a more varied behavior. Some models have average $B_{\mathrm{Dip}}/B_{\mathrm{T}}$ ratios on the order of $10^{-2}$ with minimum values on the order of $10^{-3}$ (models (5), (6) and (8)) whereas others have average ratios similar to the Earth-like cases (models (4), (7), (9), (10)). However, for some of the thinner shells with Earth-like average ratios (models (8), (10), (11)) we find the range of values obtained over the two diffusion times is larger than the range of values exhibited by the models with Earth-like shell thickness (i.e. their ratios are more variable).

The two factors that affect the $B_{\mathrm{Dip}}/B_{\mathrm{T}}$ ratio were mentioned earlier. Fig. 1 shows that for a numerical model with small $B_{\mathrm{Dip}}/B_{\mathrm{T}}$ ratio, both the $B_P/B_{\mathrm{T}}$ and the $B_{\mathrm{Dip}}/B_P$ ratios are smaller than a numerical model with Earth-like $B_{\mathrm{Dip}}/B_{\mathrm{T}}$ ratio (we use the $L_2$ norm of the poloidal field to estimate $B_{\mathrm{P}}$). Although we only plot the results for two of the models, the results are representative of all our models in Table 1. Both of these effects contribute a factor of order $10^{-1}$ to the $B_{\mathrm{Dip}}/B_{\mathrm{T}}$ ratio resulting in ratios on the order of $10^{-2}$. It therefore appears that thin shell dynamos are both

Table 1
Model parameters and results

| Model | $r_{\mathrm{io}}$ | $Ra_{\mathrm{m}}$ | $B_{\mathrm{Dip}}/B_{\mathrm{T}}$ | | | |
|---|---|---|---|---|---|---|
| | | | Mean | Median | Max | Min |
| 1 | 0.35 | 15,000 | $1.3\cdot 10^{-1}$ | $1.2\cdot 10^{-1}$ | $1.7\cdot 10^{-1}$ | $1.0\cdot 10^{-1}$ |
| 2 | 0.35 | 18,000 | $1.3\cdot 10^{-1}$ | $1.3\cdot 10^{-1}$ | $1.7\cdot 10^{-1}$ | $1.0\cdot 10^{-1}$ |
| 3 | 0.35 | 24,000 | $1.5\cdot 10^{-1}$ | $1.6\cdot 10^{-1}$ | $2.0\cdot 10^{-1}$ | $1.1\cdot 10^{-1}$ |
| 4 | 0.7 | 18,000 | $1.5\cdot 10^{-1}$ | $1.5\cdot 10^{-1}$ | $2.0\cdot 10^{-1}$ | $1.1\cdot 10^{-1}$ |
| 5 | 0.8 | 25,000 | $1.0\cdot 10^{-2}$ | $1.2\cdot 10^{-2}$ | $2.3\cdot 10^{-2}$ | $2.3\cdot 10^{-3}$ |
| 6 | 0.8 | 30,000 | $1.9\cdot 10^{-2}$ | $2.1\cdot 10^{-2}$ | $5.2\cdot 10^{-2}$ | $6.7\cdot 10^{-3}$ |
| 7 | 0.8 | 40,000 | $7.9\cdot 10^{-2}$ | $8.3\cdot 10^{-2}$ | $1.3\cdot 10^{-1}$ | $4.2\cdot 10^{-2}$ |
| 8 | 0.83 | 45,000 | $1.1\cdot 10^{-2}$ | $1.4\cdot 10^{-2}$ | $3.2\cdot 10^{-2}$ | $1.7\cdot 10^{-3}$ |
| 9 | 0.9 | 60,000 | $8.7\cdot 10^{-2}$ | $8.8\cdot 10^{-2}$ | $1.9\cdot 10^{-1}$ | $5.6\cdot 10^{-2}$ |
| 10 | 0.9 | 70,000 | $8.4\cdot 10^{-2}$ | $8.3\cdot 10^{-2}$ | $1.7\cdot 10^{-1}$ | $5.0\cdot 10^{-2}$ |

The mean, median, maximum and minimum values of the $B_{\mathrm{Dip}}/B_{\mathrm{T}}$ ratio over two magnetic diffusion times are given. We use the $L_2$ norm of the energy in the toroidal field as an estimate for $B_{\mathrm{T}}$ in the core. $B_{\mathrm{Dip}}$ is the dipole moment of the field downward projected to the core–mantle boundary (0.75 Mercury radii).

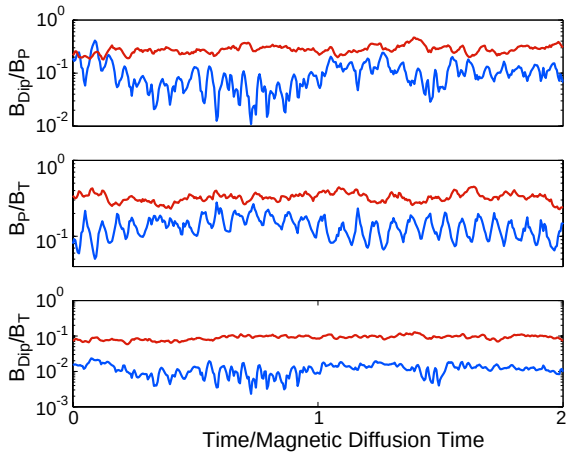


Fig. 1. Magnetic field ratios as a function of time for model (5) (blue) and model (7) (red). The ratio of the dipole field at the CMB (assumed to be at 0.75 planetary radii) to the poloidal field in the core is shown in the top plot, poloidal field to toroidal field ratio in the core is shown in the middle plot, and the ratio of dipole field at the CMB to toroidal field in the core is shown in the bottom plot. Time is given in units of magnetic diffusion time.

less efficient at producing poloidal field from toroidal field and produce smaller scale poloidal field than Earth-like models. This may not be a coincidence since perhaps poorly generated poloidal field naturally results in smaller scale structure.

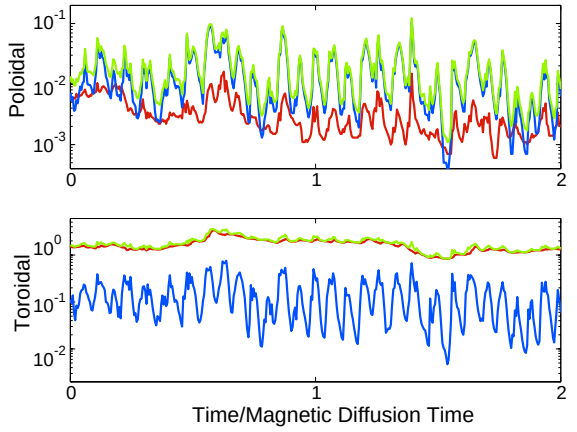


Fig. 2. Non-dimensional magnetic energy components as a function of time for model (6). The axisymmetric (red), non-axisymmetric (blue) and total (green) energy for the poloidal (top) and toroidal (bottom) fields are shown. Time is given in units of magnetic diffusion time and the energy is plotted on a log scale.

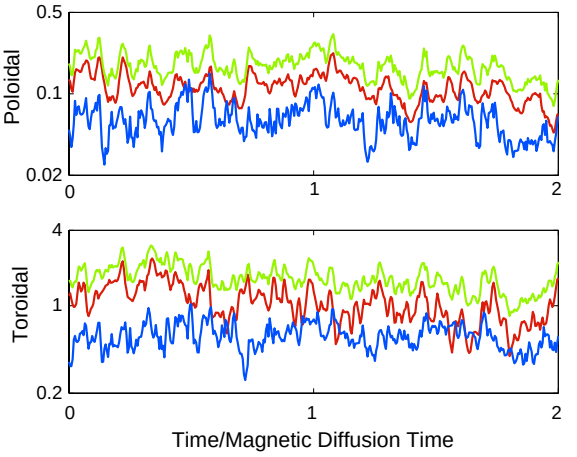


Fig. 3. Same as Fig. 2 but for model (7).

The three models with smaller $B_{\mathrm{Dip}}/B_{\mathrm{T}}$ ratios also share other similar characteristics (and differences from models with larger $B_{\mathrm{Dip}}/B_{\mathrm{T}}$ ratios). We begin by examining the energy in the fields which is defined in terms of the non-dimensional mean square field intensity:

$$E = E_{\mathrm{BT}} + E_{\mathrm{BP}} = \int_v |\mathbf{B}_{\mathrm{T}}|^2 \mathrm{d}V + \int_v |\mathbf{B}_{\mathrm{P}}|^2 \mathrm{d}V, \quad (12)$$

where $E_{\mathrm{BT}}$ and $E_{\mathrm{BP}}$ are the energy in the toroidal and poloidal fields, respectively, and $V$ is the non-dimensional volume of the fluid outer core. In Figs. 2 and 3

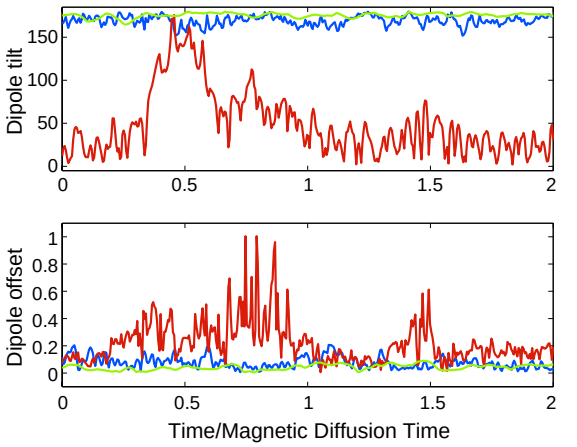


Fig. 4. Eccentric dipole models as a function of time. Dipole tilt (top) and offset (bottom) are shown for models (1) (green), (5) (blue) and (7) (red). Time is given in units of magnetic diffusion time and dipole offset is in units of planetary radii.

we compare the partitioning of poloidal and toroidal energy in the core into axisymmetric and non-axisymmetric components for models (6) and (7), respectively. These models have the same $r_{io}$ value but model (6) has a small $B_{Dip}/B_T$ ratio and model (7) has an Earth-like $B_{Dip}/B_T$ ratio. The model with smaller $B_{Dip}/B_T$ ratio has a poloidal energy dominated by the non-axisymmetric component and toroidal energy dominated by the axisymmetric component. In contrast, the Earth-like $B_{Dip}/B_T$ ratio model has both poloidal and toroidal energy dominated by the axisymmetric component. The dominant axisymmetric toroidal energy in both models is not surprising since it is generated through the shearing action of differential rotation which is present in both cases. The difference in poloidal energy dominance suggests that the mechanism generating poloidal field behaves differently in the two models. The non-dimensionalization of magnetic field in our model implies that when $|\mathbf{B}|=1$, the ratio of Lorentz to Coriolis forces is 1 (in other words the Elsasser number $\Lambda=1$). Figs. 2 and 3 therefore also demonstrate that our models are in the magnetostrophic balance regime where $\Lambda \sim O(1)$.

Another characteristic we can compare is eccentric dipole models. Fig. 4 plots the eccentric dipole

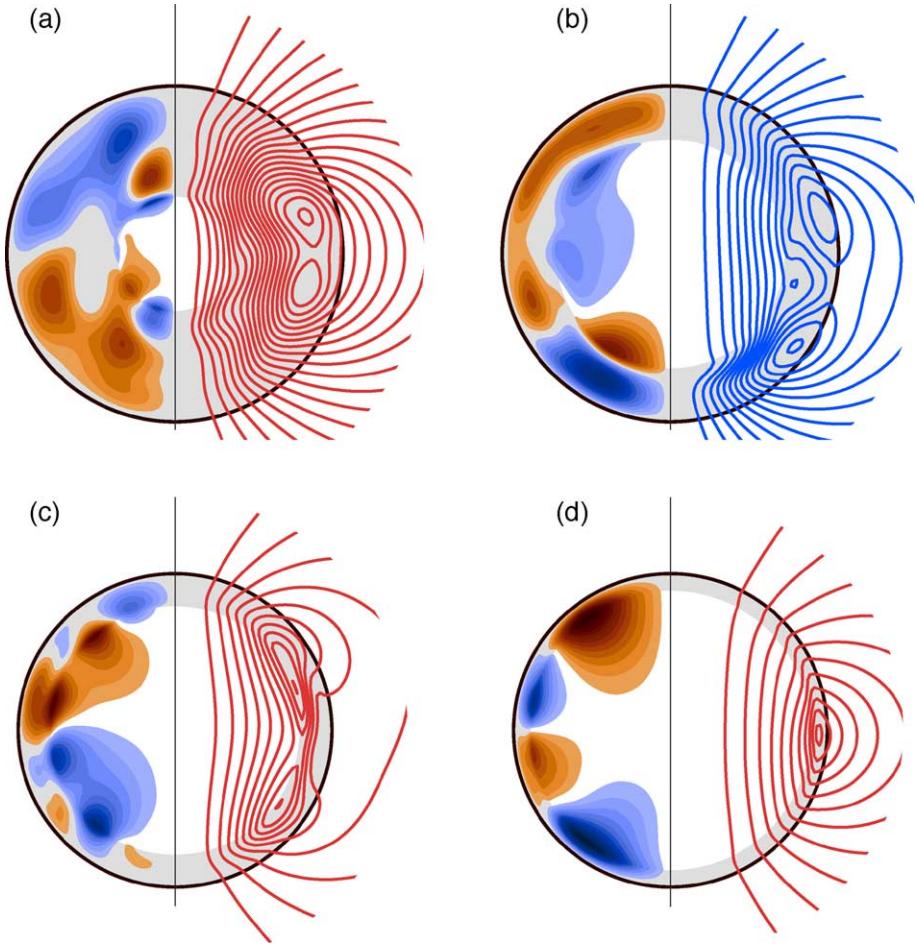


Fig. 5. Axisymmetric magnetic field at one instant in time for models (2) (a), (4) (b), (7) (c) and (9) (d). Contours of the toroidal field are shown in the left half and streamlines of the poloidal field are shown in the right half of the plots. The different colors represent different field directions. The gray shell is the fluid core, the inner white region is the solid inner core, the thick black circle is the CMB and the black vertical line represents the rotation axis.

tilts and offsets for models (1), (5) and (7). The model with small $B_{Dip}/B_T$ ratio experiences larger variations in dipole tilt and offset than the thin shell model with Earth-like $B_{Dip}/B_T$ ratio and the thick-shell Earth-like model. These results are characteristics of the other models in Table 1 that have similar $B_{Dip}/B_T$ ratios. The larger eccentric dipole tilts and offsets of models with small $B_{Dip}/B_T$ ratio do not only occur during reversals (as the one shown in Fig. 4), but also during times of stable polarity direction. Only two of the three small $B_{Dip}/B_T$ ratio models in Table 1 underwent a reversal at some point during the two diffusion times studied, however all three demonstrated similar variability in dipole tilt and offset when not reversing.

Although some of the thin shell models produce Earth-like $B_{Dip}/B_T$ ratios, there are differences between the fields generated by these dynamos and thick shell dynamos. Fig. 5 compares the axisymmetric toroidal and poloidal fields in models with various shell thicknesses, but Earth-like $B_{Dip}/B_T$ ratios. The dominant pattern of toroidal magnetic field changes as the shell thickness varies. The thick-shell model in Fig. 5a is dominated by a spherical harmonic degree 2 pattern which remains relatively stable in time. In contrast, the very thin-shell model in Fig. 5d is dominated by a degree 4 pattern in both the time-averaged field and at the time step shown, however this model can also display a more complex toroidal field with contributions from multiple spherical harmonic degrees at certain times. For intermediate shell thicknesses (Fig. 5b, c) the pattern appears to be going through a transition between the two states and therefore contains more complicated structure with significant contributions from both degree 2 and 4 components. The change to higher-degree (smaller scale) structure as the shell thickness decreases is perhaps not surprising since a length-scale in the problem is becoming smaller, however it is interesting that these different toroidal field morphologies still produce a dominant dipolar poloidal field.

We can also compare model (7)'s axisymmetric magnetic field (Fig. 5c) to that of model (6) (Fig. 6), which has the same shell thickness but a small $B_{Dip}/B_T$ ratio. Although the shell thickness is the same, the toroidal field patterns in these models are different. In model (6) the axisymmetric toroidal field is concentrated inside the tangent cylinder whereas in model (7) the toroidal field is found throughout the fluid core.

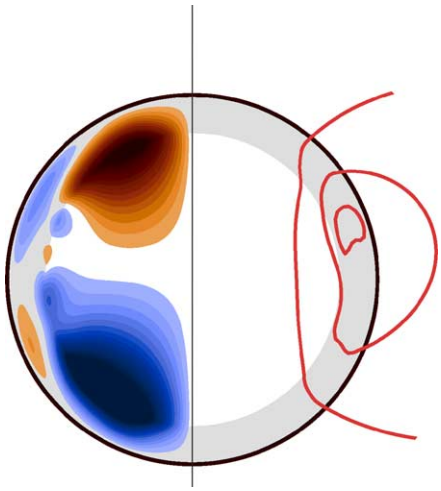

Fig. 6. Same as Fig. 5 but for model (6).

## 5. Discussion

The purpose of this study was to determine the existence of numerical dynamos with non-Earth-like $B_{Dip}/B_T$ ratios, and this was accomplished, but our search of parameter space was not complete enough to determine the specific dependence of the $B_{Dip}/B_T$ ratio on shell thickness and modified Rayleigh number. We do however, observe some trends that will be verifiable once a further study of parameter space has been conducted.

Models (5)–(7) have the same inner core radius ($r_{io}=0.8$) but different modified Rayleigh numbers. The results suggest that lower modified Rayleigh numbers are able to produce fields with smaller $B_{Dip}/B_T$ ratios. When we lowered the modified Rayleigh number to $Ra_m=20\,000$ for the same shell thickness, the strong field dynamo solution died. This suggests that modified Rayleigh numbers in a limited region near the lower boundary for strong field dynamo action in our numerical models can produce smaller $B_{Dip}/B_T$ ratios. In future work we will examine whether this trend prevails at other inner core radii. The two models with $r_{io}=0.9$ (models (9) and (10)) produce Earth-like ratios at

their modified Rayleigh numbers. In a model with the same inner core radius and $Ra_m = 30\,000$ we found the strong-field dynamo died. If dynamos operating at this shell thickness can produce smaller $B_{Dip}/B_T$ ratios, our results from the $r_{io} = 0.8$ case suggest it will occur somewhere in the $Ra_m$ range of 30 000–60 000. This trend does not appear to occur for Earth-like shell thicknesses since model (1) which has an Earth-like $B_{Dip}/B_T$ ratio has a modified Rayleigh number very close to the critical value for strong field dynamo action [20]. This suggests that the field partitioning has a dependence on shell thickness as well as on modified Rayleigh number. Determining the critical shell thickness for which this trend begins to appear will be the goal of future parameter space searches.

Now that the existence of numerical dynamos with Mercury-like $B_{Dip}/B_T$ ratios has been established, we examine the cause of this different field morphology. As a consequence of the Proudman-Taylor theorem [22,23], the convection pattern in a spherical rapidly rotating shell is dominated by 2-dimensional columnar rolls [24,25] that form parallel to the rotation axis outside the tangent cylinder (cylinder coaxial with rotation axis and tangent to the inner core boundary). Convection inside the tangent cylinder is more difficult since the geometry requires the complex 3-D motions that transfer heat from the inner core boundary to the CMB to break the 2-dimensionality imposed by the Proudman-Taylor theorem. In a thick shell geometry, these convection columns are an efficient means of producing poloidal magnetic field from toroidal field since the region outside the tangent cylinder occupies a large fraction of the fluid core's volume and the toroidal field is present throughout this region. However, as the shell thickness decreases, the region outside the tangent cylinder occupies a smaller ratio of the total volume and therefore, the convective motions outside the tangent cylinder do not interact as efficiently with the toroidal field which is present in the entire fluid shell. The ratio of magnetic field generation to dissipation is given by the magnetic Reynolds number ($Re_M$). As the shell thickness decreases, the velocity (i.e. the convective vigor) must increase in order to maintain the same level of field generation (same $Re_M$). One might expect that at a certain shell thickness, the Rayleigh numbers required to maintain strong field dynamo action outside the tangent cylinder may be similar to those for the onset of dynamo action inside the tangent cylinder.

We can now provide a possible explanation for both the shell thickness and Rayleigh number dependencies seen in our models. The toroidal field is generated efficiently in both thick and thin shells through differential rotation ($\omega$ effect). The poloidal field is generated when upwellings from convection produce poloidal field from toroidal field (macroscopic $\alpha$ effect). In our numerical thick shell dynamos these processes result in a $B_{Dip}/B_T$ ratio of about $10^{-1}$. As the shell thickness decreases, columnar convection becomes less efficient at producing poloidal field from toroidal field because the columns occur in a limited region outside the tangent cylinder. We obtain dynamos with small $B_{Dip}/B_T$ ratios in the parameter regime when convection outside the tangent cylinder is not efficient at producing poloidal field (i.e. thin shells) and the modified Rayleigh number is low enough that convection inside the tangent cylinder does not efficiently produce poloidal field. We obtain Earth-like $B_{Dip}/B_T$ ratios in thin shell geometries when the Rayleigh number is large enough that convection inside the tangent cylinder is capable of producing a strong poloidal field from the strong toroidal field there. This is why models (5) and (6) have small $B_{Dip}/B_T$ ratios whereas model (7), which has the same shell thickness but larger modified Rayleigh number, has an Earth-like $B_{Dip}/B_T$ ratio. Small $B_{Dip}/B_T$ ratios may no longer occur in dynamos when the shell thickness is small enough that either convection outside the tangent cylinder alone is not efficient enough to produce dynamo action (can't get to critical $Re_M$), or dynamo action inside and outside the tangent cylinder occur at similar critical Rayleigh numbers. At this point the convection inside the tangent cylinder will be an efficient means of producing poloidal field and Earth-like $B_{Dip}/B_T$ ratios will result. A sketch of these different scenarios is shown in Fig. 7.

We see evidence of this process occurring in our dynamo models. In Figs. 8 and 9 we show the non-axisymmetric component of the axial vorticity of the fluid flow in slices parallel to the equator for models (5) and (7), respectively. The slices in the

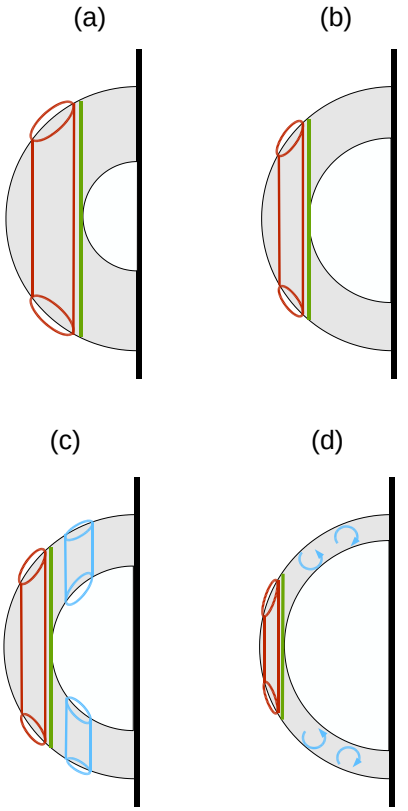


Fig. 7. Sketch of theoretical convective flow patterns in meridional slices for models with varying shell thicknesses. The black and green lines represent the rotation axis and tangent cylinder respectively, gray regions are the fluid outer core and inner white regions are the solid inner core. A thick shell geometry (a) has a convection pattern dominated by columnar rolls (red cylinders) that form near the tangent cylinder. This form of convection is efficient at generating poloidal dipolar field and produces Earth-like $B_{\mathrm{Dip}}/B_{\mathrm{T}}$ ratios. As shell thickness decreases, the convection columns become shorter and move to regions of higher boundary slope. If the Rayleigh number is low enough so that convection does not occur inside the tangent cylinder, then these rolls are not efficient at converting toroidal field to poloidal dipole field (b) and these dynamos can produce smaller $B_{\mathrm{Dip}}/B_{\mathrm{T}}$ ratios. At similar shell thicknesses but higher Rayleigh numbers, convection inside the tangent cylinder is more efficient at producing poloidal dipole field (c) causing Earth-like $B_{\mathrm{Dip}}/B_{\mathrm{T}}$ ratios. Eventually a shell thickness may be reached where convection inside and outside the tangent cylinder begin at similar critical Rayleigh numbers, eliminating the small $B_{\mathrm{Dip}}/B_{\mathrm{T}}$ ratio regime (d).

equatorial plane (part (a) in both figures) contain similar convection patterns occurring outside the tangent cylinder, however model (7) convects more vigorously as expected since the modified Rayleigh number is larger in this model. In part (b) of both figures, we plot the convection pattern in a plane parallel to the equatorial plane at a height of $z=0.4r_{\mathrm{o}}$.

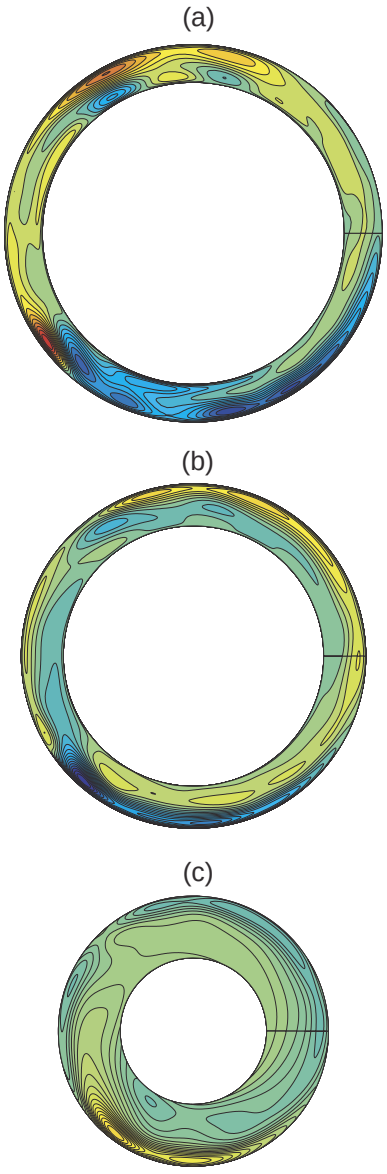


Fig. 8. The axial vorticity of the non-axisymmetric poloidal velocity field in slices parallel to the equatorial plane for model (5). A slice through the equatorial plane is shown in (a), a slice through a plane parallel to the equator at a height of 0.4 $r_{\mathrm{o}}$, is shown in (b) and at a height of 0.7 $r_o$ is shown in (c). The color scale is the same in all plots to give an idea of differences in magnitude. The contour lines scale differently between plots to give a better idea of structure in each plot.

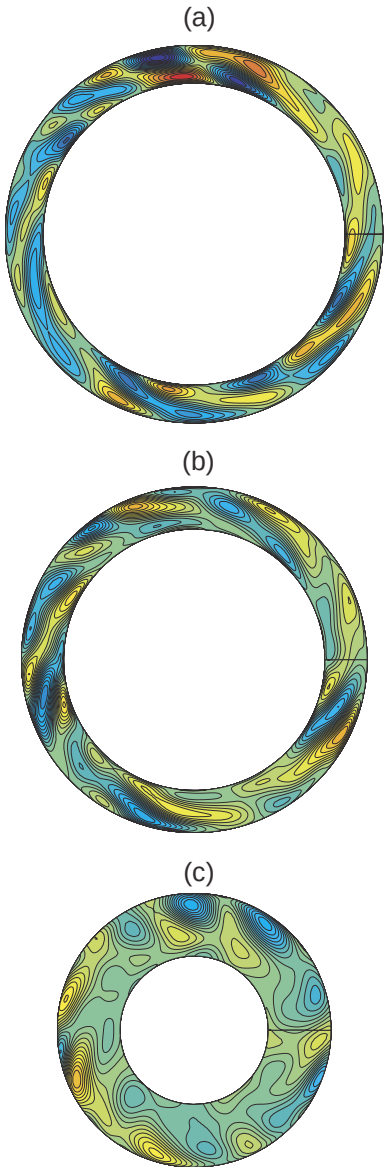


Fig. 9. Same as Fig. 8 but for model (7). The color scale in the figure is also the same as in Fig. 8 in order to compare intensities between models.

Here we see that model (7) has much stronger, smaller scale convection patterns than model (5). In part (c) of both figures, the convection pattern in a plane parallel to the equator at a height of $z=0.7r_o$ is shown. In model (5) at lower Rayleigh number (Fig. 8), convection is weak or absent inside the tangent cylinder whereas at higher Rayleigh number (Fig. 9), we see the stronger convection patterns inside the tangent cylinder.

## 6. Conclusions

We have demonstrated that dynamos operating in thin shells can produce a variety of behaviors not seen in thick-shell dynamos. Further study of this geometry is necessary for understanding the magnetic field generation process in planets and may be relevant for Mercury as well as Ganymede and perhaps Mars' past dynamo. Al-Shamali et al. [26] have recently performed numerical studies of the onset of convection in thin shells and Aurnou et al. [27] have performed experiments on convection patterns inside the tangent cylinder. Both of these forms of study, along with numerical dynamo studies will be important in understanding dynamo generation in thin shells. In future work we will explore more of parameter space in our numerical models to determine the dependence of this new field morphology on the governing parameters.

This first study has shown that a dynamo solution for Mercury's magnetic field is possible since thin shell dynamos can produce fields with Mercury-like partitioning of toroidal and poloidal fields, however, it does not rule out crustal magnetization or a thermoelectric dynamo as the source of Mercury's field. Future measurements of Mercury's magnetic field by the MESSENGER and Bepi-Colombo missions may help to resolve the issue. If any field variability in time is observed, then the dynamo source will prove correct. If the field structure is correlated with gravity signatures indicating topography at the core–mantle boundary then a thermoelectric dynamo will be the most likely answer. Any small-scale structure with shallow source depths is crustal in origin. If no time-variation is detected this does not mean the field is not dynamo generated, just that the timescale of secular variation is longer than the length of time the observations are carried out. Determining whether the field is crustal or dynamo generated in this case may be possible if evidence of an effect due to the tangent cylinder is seen. If the character of the magnetic field is different inside and outside the tangent cylinder (due to different convection

patterns in these regions) then a dynamo source for the field may be the answer.

## Acknowledgments

Sabine Stanley was partly funded by the National Science and Engineering Research Council of Canada (NSERC). We wish to thank David Stevenson and Julien Aubert for helpful reviews of the manuscript.

## References

[1] N.F. Ness, K.W. Behannon, R.P. Lepping, Y.C. Whang, The magnetic field of Mercury, 1, J. Geophys. Res. 80 (1975) 2708–2716.
[2] N.F. Ness, K.W. Behannon, R.P. Lepping, Y.C. Whang, Observations of Mercury's magnetic field, Icarus 28 (1976) 479–488.
[3] J.E.P. Connerney, N.F. Ness, Mercury's magnetic field and interior, in: F. Vilas, C.R. Chapman, M.S. Matthews (Eds.), Mercury, University of Arizona Press, Tucson, AZ, 1988, pp. 494–513.
[4] S. Runcorn, An ancient lunar magnetic field, Nature 253 (1975) 701–703.
[5] A. Stephenson, Crustal remanence and the magnetic moment of Mercury, Earth Planet. Sci. Lett. 28 (1975) 454–458.
[6] L. Srnka, Magnetic dipole moment of a spherical shell with TRM acquired in a field of internal origin, Phys. Earth Planet. Inter. 11 (1976) 184–190.
[7] O. Aharonson, M.T. Zuber, S.C. Solomon, Crustal remanence in an internally magnetized non-uniform shell: a possible source for Mercury's magnetic field? Earth Planet. Sci. Lett. 218 (2004) 261–268.
[8] M. Kivelson, K. Khurana, C. Russell, R. Walker, J. Warnecke, F. Coroniti, C. Polanskey, D. Southwood, G. Schubert, Discovery of Ganymede's magnetic field by the Galileo spacecraft, Nature 384 (1996) 537–541.
[9] J. Margot, S. Peale, R.F. Jurgens, M.A. Slade, I.V. Holin, Earth-based measurements of Mercury's forced librations in longitude, Eos Trans. AGU 85 (2004) GP33-03.
[10] R.W. Siegfried, S.C. Solomon, Mercury: internal structure and thermal evolution, Icarus 23 (1974) 192–205.
[11] D.J. Stevenson, T. Spohn, G. Schubert, Magnetism and thermal evolution of the terrestrial planets, Icarus 54 (1983) 466–489.
[12] G. Schubert, M.N. Ross, D.J. Stevenson, T. Spohn, Mercury's thermal history and the generation of its magnetic field, in: F. Vilas, C.R. Chapman, M.S. Matthews (Eds.), Mercury, University of Arizona Press, Tucson, AZ, 1988, pp. 429–460.
[13] V. Conzelmann, T. Spohn, New thermal evolution models suggesting a hot, partially molten Mercurian interior, Bull.-Am. Astron. Soc. 31 (1999) 1102.
[14] S. Hauck, A. Dombard, R. Phillips, S. Solomon, Internal and tectonic evolution of Mercury, Earth Planet. Sci. Lett. 222 (2004) 713–728.
[15] D.J. Stevenson, Mercury's magnetic field: a thermoelectric dynamo? Earth Planet. Sci. Lett. 82 (1987) 114–120.
[16] G. Giampieri, A. Balogh, Mercury's thermoelectric dynamo model revisited, Planet. Space Sci. 50 (2002) 757–762.
[17] D.J. Stevenson, The energy flux number and three types of planetary dynamo, Astron. Nachr. 305 (1984) 257–264.
[18] C. Kutzner, U.R. Christensen, From stable dipolar towards reversing numerical dynamos, Phys. Earth Planet. Inter. 131 (2002) 29–45.
[19] W. Kuang, J. Bloxham, An Earth-like numerical dynamo model, Nature 389 (1997) 371–374.
[20] W. Kuang, J. Bloxham, Numerical modeling of magneto-hydrodynamic convection in a rapidly rotating spherical shell: weak and strong field dynamo action, J. Comp. Phys. 153 (1999) 51–81.
[21] J. Bloxham, S. Zatman, M. Dumberry, The origin of geo-magnetic jerks, Nature 420 (2002) 65–68.
[22] J. Proudman, On the motions of solids in a liquid possessing vorticity, Proc. R. Soc. Lond., A 92 (1916) 418–424.
[23] G.I. Taylor, Motion of solids in fluids when the flow is not irrotational, Proc. R. Soc. Lond., A 93 (1917) 99–113.
[24] F.H. Busse, Thermal instabilities in rapidly rotating systems, J. Fluid Mech. 44 (1970) 441–460.
[25] F.H. Busse, Convective flows in rapidly rotating spheres and their dynamo action, Phys. Fluids 14 (2002) 1301–1314.
[26] F.M. Al-Shamali, M.H. Heimpel, J.M. Aurnou, Varying the spherical shell geometry in rotating thermal convection, Geophys. Astrophys. Fluid Dyn. 98 (2004) 153–169.
[27] J. Aurnou, S. Andreadis, L. Zhu, P. Olson, Experiments on convection in Earth's core tangent cylinder, Earth Planet. Sci. Lett. 212 (2003) 119–134.